Effect of Inorganic Phosphate on the Force and Number of Myosin Cross-Bridges During the Isometric Contraction of Permeabilized Muscle Fibers from Rabbit Psoas

Marco Caremani,*† Jody Dantzig,‡ Yale E. Goldman,‡ Vincenzo Lombardi,*§ and Marco Linari*†
*Laboratorio di Fisiologia, DBE, and †CNISM, Università di Firenze, Florence, Italy; ‡Department of Physiology, University of Pennsylvania, Philadelphia, Pennsylvania; and §CRS SOFT-INFM-CNR, Università di Roma "La Sapienza", Rome, Italy

ABSTRACT The relation between the chemical and mechanical steps of the myosin-actin ATPase reaction that leads to generation of isometric force in fast skeletal muscle was investigated in demembranated fibers of rabbit psoas muscle by determining the effect of the concentration of inorganic phosphate (Pi) on the stiffness of the half-sarcomere (hs) during transient and steady-state conditions of the isometric contraction (temperature 12°C, sarcomere length 2.5 μm). Changes in the hs strain were measured by imposing length steps or small 4 kHz oscillations on the fibers in control solution (without added Pi) and in solution with 3–20 mM added Pi. At the plateau of the isometric contraction in control solution, the hs stiffness is 22.8 $\pm$ 1.1 kPa nm^{-1}. Taking the filament compliance into account, the total stiffness of the array of myosin cross-bridges in the hs (e) is 40.7 $\pm$ 3.7 kPa nm^{-1}. An increase in [Pi] decreases the stiffness of the cross-bridge array in proportion to the isometric force, indicating that the force of the cross-bridge remains constant independently of [Pi]. The rate constant of isometric force development after a period of unloaded shortening (r_F) is 23.5 $\pm$ 1.0 s^{-1} in control solution and increases monotonically with [Pi], attaining a maximum value of 48.6 $\pm$ 0.9 s^{-1} at 20 mM [Pi], in agreement with the idea that Pi release is a relatively fast step after force generation by the myosin cross-bridge. During isometric force development at any [Pi], e and thus the number of attached cross-bridges increase in proportion to the force, indicating that, independently of the speed of the process that leads to myosin attachment to actin, there is no significant (>1 ms) delay between generation of stiffness and generation of force by the cross-bridges.

INTRODUCTION

Force and shortening in striated muscle are generated by the myosin II molecular motors working in parallel in each half of the thick filament. The globular S1 portion of the myosin molecule, the myosin head (M), cyclically attaches to an actin site (A) on the thin filament and undergoes a structural working stroke based on the energy released by the hydrolysis of one ATP molecule (1). The currently available description of the coupling between biochemical and structural changes in the myosin cross-bridge from skeletal muscle (2,3) provides that the structural changes during the working stroke that is responsible for the 10 nm reciprocal sliding between the myosin and actin filaments consists of a 70° tilting of the light chain domain (LCD) of the myosin head about a fulcrum in the catalytic domain (CD). The working stroke is associated with the release of the hydrolysis product orthophosphate (Pi) and a further contribution is provided by the subsequent release of ADP (4).

In Ca^{2+}-activated skinned muscle fibers, the addition of Pi has been found to reduce the isometric force (T_0) (5–14) and increase the kinetics of cross-bridge interactions after photolysis of caged ATP starting from rigor (7). Accordingly, the rate constant of isometric force development increases at higher [Pi] (12,15,16). Also, the rate constant of the force transient elicited by a jump in [Pi] superimposed on steady isometric force increases with [Pi] (12,14,15,17–20). With one exception (21), all previous studies reported that fiber stiffness is reduced in the presence of Pi to a lesser extent than isometric force (8,14,15,17–20). In view of the fact that fiber stiffness can be used to estimate the number of attached cross-bridges, these results were interpreted as showing that the Pi release step is associated with the transition to higher force generating states of the attached cross-bridges. Under this hypothesis, the increase of the apparent reverse rate constant of the transition on increase of [Pi] shifts the distribution toward a cross-bridge state that exerts low or no force (8,14,15). At the same time, the finding that 1), the reduction in isometric force; 2), the increase of the rate constant of force development; and 3), the increase of the rate constant of the force transient elicited by Pi jump all saturate at high [Pi] suggests that the force in the attached myosin head is generated before Pi release (14,15,18,19,21,22). All of these results are accounted for by a six-step reaction pathway for the myosin-actin ATPase cycle (15) (see Scheme 1).

According to this scheme, the weakly bound A-M.ADP.Pi cross-bridge isomerizes to form an AM*.ADP.Pi cross-bridge bearing stiffness but no force (step 3), before the transition to the force bearing AM'.ADP.Pi cross-bridge (step 4). Pi is rapidly released afterward (step 5) without further enhancement of force generation. A chemomechanical cycle, including an actin-attached zero force state of the cross-bridge with the hydrolysis products still bound in the catalytic site, was also used to explain that the rate constant of the force

Submitted January 27, 2008, and accepted for publication June 12, 2008.

Address reprint requests to Marco Linari, E-mail: marco.linari@unifi.it.

Editor: Shin'ichi Ishiwata.

0006-3495/08/12/5798/11 $2.00

doi: 10.1529/biophysj.108.130435

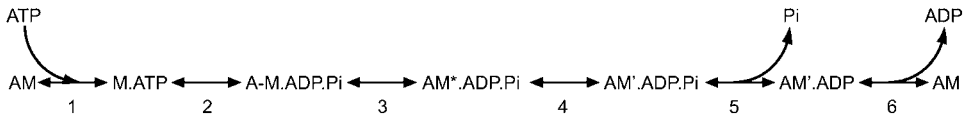

Scheme 1

development after unloaded shortening is lower than the rate constant of the force transient elicited by a Pi jump (12,15,17–19). In fact, according to the scheme assumed by Regnier et al. (15), although the rate of the force transient after a Pi jump is kinetically controlled by step 4, the rate of force development is kinetically controlled by steps 3 and 4. However, the slower rate of the de novo force generation could equally be accounted for by assuming, in agreement with solution kinetic measurements, a lower rate for the ATP hydrolysis (step 2) (23).

The growing evidence that a substantial fraction of the elasticity present in the half-sarcomere (hs) is due to the compliance of the myofilaments (24–30) implies that the reduction of the number of attached cross-bridges by Pi is underestimated by the change of the fiber stiffness, and that the stoichiometry and kinetics of the reaction cycle may need revision. A precise estimate of the occupancy of the relevant states of the cross-bridges, with definitions of their chemical and mechanical identities, is indispensable to describe in detail the reaction kinetics of the myosin cross-bridge with actin in situ in the isometric contraction. By applying fast-sarcomere-level mechanics to demembranated fibers from rabbit psoas (31,32), we recently demonstrated that the cross-bridges responsible for the isometric force at saturating pCa are ~1/3 of the total present in each hs (30).

In the work presented here, we reinvestigate the effects of Pi on the distribution of myosin cross-bridges through the various states of the reaction cycle and on their mechanical characteristics during transient and steady-state conditions imposed on isometric contractions. The results show that the mass action of [Pi] reduces the number of actin-attached cross-bridges responsible for stiffness and the force by the same amount, so that the average force per cross-bridge is not altered by the level of Pi. Thus the kinetic relevance of the AM*.ADP.Pi state (15) is negligible and force generation by the cross-bridges is synchronous with the transition from the weakly bound to the strongly attached state (e.g., step 3 in the scheme above).

MATERIALS AND METHODS

Experiments were initiated at the University of Pennsylvania and completed at the University of Florence. Except where indicated, the methods described below refer to experiments or procedures used at both locations.

Experiments were done on glycerinated skinned fiber segments from psoas muscles of adult male New Zealand white rabbits (3–5 kg). The rabbits were killed in accordance with the official regulations of the community council on the use of laboratory animals, and the study was approved by the ethics committee for animal experiments. Single fibers were prepared as previously described (30,33). A fiber segment, 5–6 mm long, was cut from the fiber and T-shaped aluminum clips were mounted at its extremities for attachment to transducer hooks. To minimize the shortening of the fiber segment by extension of the damaged extremities and the development of inhomogeneity in sarcomere length across the fiber, the two ends of the fiber were fixed with glutaraldehyde in rigor solution before they were clamped by the aluminum clips. At the University of Florence, the glutaraldehyde-fixed ends of the fiber segment were also glued to the clips with shellac dissolved in ethanol (29).

Experimental setup

The fiber was mounted in a drop of relaxing solution between the lever arms of a loudspeaker motor, in a manner similar to that described by Lombardi and Piazzesi (34), and a force transducer. The force transducers were either a strain gauge transducer (AE801 (SensoNor, Horten, Norway), sensitivity 10–20 VN^{-1} and resonant frequency 2.3–11.3 kHz) or a capacitance transducer (sensitivity 80–200 VN^{-1}, resonant frequency 40–50 kHz (35)). The capacitance force transducer was used for experiments in which 4 kHz oscillations were imposed on the fiber for stiffness measurements.

At the University of Pennsylvania, an assembly with six troughs was used for rapid exchange of solutions (33). During activation the striation spacing of a central region of the fiber (~1.8 mm) was monitored at high resolution using a white-light diffractometry system that avoids the Bragg-angle artifact observed in laser diffraction experiments (36). At the University of Florence, the solution exchange system allowed continuous recording of length changes of a selected population of sarcomeres (500–1200) by a striation follower (37). In this system, most of the force develops in the activating solution after a rapid rise in temperature (T-jump) from 1°C to the test temperature (29,30). In the fibers selected for this work, the amount of shortening per hs to attain the isometric force was <35 nm.

Experimental protocol

After the fiber was mounted on the transducer levers, the sarcomere length (*sl*), width (*w*), and height (*h*) were measured at 0.5 mm intervals in the 3–4 mm central segment of the relaxed fiber with a 40× dry objective (Zeiss, NA 0.60) and a 25× eyepiece. The fiber length (L_0) was set so that *sl* was 2.48 ± 0.05 μm (mean ± SD). The fiber cross-sectional area (CSA), determined assuming the fiber cross-section is elliptical, was ($\pi/4 \cdot w \cdot h =$) 4300 ± 1300 μm^2.

Experiments were performed at 10–12°C. The experimental protocols described below were used to investigate the effect of Pi on the kinetics and mechanics of the myosin-actin interaction.

Stiffness measurements during the isometric contraction at different [Pi] values

Step releases and stretches (rise time ~110 μs, amplitude range ±3 nm) were applied during the isometric contraction of fibers activated with saturating Ca^{2+} both in control solution (without added Pi) and in test solution (range of [Pi] 3–25 mM). The stiffness of the hs was estimated by the slope of the relation between tension attained at the end of the step and the size of the step in hs length (T_1 relation (38)). In five of the nine fibers used, measurements were done only with 0 and 10 mM added Pi. These experiments used the more recent activation technique developed at the University of Florence, and the isometric force and stiffness values at the same [Pi] were slightly higher than those of fibers from the earlier experiments made at the University of Pennsylvania (see Table 2). However, the analysis of the hs sarcomere elasticity to identify the contribution of the myofilaments and the cross-bridges gave similar results, and the data from the two sets of experiments were merged.

Development of isometric force and stiffness after unloaded shortening

The time course of development of force and hs stiffness was measured after a period of unloaded shortening, obtained by imposing a fast shortening ramp (amplitude ~5% of the fiber length, duration 3 ms) on the isometrically activated fibers. The hs stiffness was determined by imposing 4 kHz length oscillations (amplitude peak-to-peak ≤0.2% L_0) both on the plateau of the isometric force (T_0) just before the period of unloaded shortening and during force development between 0.25 and 0.9 T_0. The stiffness was estimated by the ratio of the force change to the change in hs length recorded from a fiber segment, the average position of which was 1.2–1.4 mm from the force transducer end. In this way, the propagation time of the mechanical perturbation and thus the lag between length and force signals were minimized and there was no significant contribution from out-of-phase stiffness. The analysis was done on 80 cycles every 20 ms by means of a fast Fourier transform routine (LabVIEW software, National Instruments, Austin, TX) to estimate the in-phase and out-of-phase stiffness. The maximum force increase in the 20 ms period was ~0.1 T_0 at the start of the oscillation period. The analysis of the rate of force development was executed in eight fibers both in the absence of added Pi and in test solution ([Pi] 10 mM). In three of the eight fibers the range of [Pi] was extended from 3 to 20 mM. The analysis of the stiffness change during force development at 0 and 10 mM added Pi was executed in three fibers.

Data collection and analysis

Force, motor position, and sarcomere length signals were recorded with a multifunction I/O board (PCI-6110E, National Instruments), and a dedicated program written in LabVIEW (National Instruments) was used for signal recording and analysis. Data are expressed as mean ± SE except for the CSA and *sl* (mean ± SD).

Analysis of force development

The time course of force development after unloaded shortening was quantified by fitting with the biexponential equation:

$$T_r = T_F(1 - \exp(-r_F t)) + T_S(1 - \exp(-r_S t)), \quad (1)$$

where t is the time elapsed from the start of force development after the end of shortening estimated by back-extrapolation of the force response; T_r is the force response; T_F and T_S are the amplitudes of the fast and slow exponentials, respectively; and r_F and r_S are the rate constants of the fast and slow exponentials, respectively.

The set of coefficients that best fit the trace by least-squared residuals was determined by means of the Levenberg-Marquardt algorithm running in LabVIEW. The quality of the fit did not improve by increasing the number of exponentials in Eq. 1; adding a third exponential reduced the residuals by <0.1%. In the fibers selected for this work, under all conditions, the amplitude of the slow exponential component is always <40% of the amplitude of the fast exponential component. The origin of the slow component is not clear; it may depend on the creep in force due to residual inhomogeneity developing among sarcomeres with the rise of force. Whatever its origin, its extent does not vary with the protocols used, so the slow component does not influence the kinetic analysis of the main component.

Solutions and Pi concentration

The composition of the solutions (Table 1 *A*) was determined with the use of a program similar to those previously described (33,39). The starting Pi concentration was adjusted by adding KH_2PO_4 and reducing the concentration of Na_2CP and EGTA/CaEGTA to achieve the same ionic strength as the control solution (no added Pi) (Table 1 *B*). As previously reported (11), the control solution without added Pi should contain ~1 mM Pi from two sources: Pi contamination in the experimental buffer and accumulation of Pi inside the fiber during contraction.

TABLE 1 Composition of solutions

(*A*) Solutions used in control (0 added Pi)

	Na_2ATP	$MgCl_2$	EGTA	HDTA	CaEGTA	TES	Na_2CP	GSH
Relaxing	5.4	7.7	25	—	—	100	19.1	10
Preactivating	5.5	6.9	0.1	24.9	—	100	19.5	10
Activating	5.5	6.8	—	—	25	100	19.5	10

(*B*) Activating solutions at different [Pi]

Added [Pi]	Na_2ATP	$MgCl_2$	CaEGTA	TES	Na_2CP	GSH
0	5.49	6.8	25	100	19.5	10
3	5.49	6.8	23	100	20.5	10
5	5.49	6.9	20	100	21.4	10
10	5.49	6.9	15	100	23.3	10
15	5.49	7.0	10	100	26.7	10
20	5.49	7.0	5	100	27.0	10
25	5.49	6.9	4	100	26.0	10

(*A*) Composition of all solutions in control (no added Pi). (*B*) Activating solutions containing different Pi concentrations. The composition of relaxing and preactivating solutions with different Pi concentrations was changed accordingly and is not reported in the table. All concentrations are in mM. ATP, adenosine 5′-triphosphate; EGTA, ethylene glycol-bis-(β-aminoethyl ether)-*N*,*N*,*N*′,*N*′-tetraacetic acid; HDTA, 1,6 diaminohexane-*N*,*N*,*N*′,*N*′-tetraacetic acid; TES, *N*-tris[hydroxymethyl]methyl-2-aminoethanesulphonic acid; CP, *N*-[Imino(phosphonoamino) methyl]-*N*-methylglycine; GSH, glutathione. 1 mg ml^{-1} creatine phosphokinase, 10 μM trans-epoxysuccinyl-L-leucylamido-(4-guanidino)butane (E-64) and 20 μg ml^{-1} leupeptin, were added to all solutions. In all solutions, ionic strength ranged between 188 and 195 mM, free Mg^{2+} was 1.3 mM and MgATP was 5 mM. In activating solutions pCa ranged between 4.8 and 4.4. pH (adjusted with KOH) was 7.1 at 12°C. HDTA was obtained from Fluka (Buchs, Switzerland); all other chemicals were obtained from Sigma (St. Louis, MO).

RESULTS

Half-sarcomere stiffness and cross-bridge stiffness in isometric contraction at different Pi concentrations

In Fig. 1 are shown the force responses to step changes in hs length (range ± 3 nm) superimposed on the plateau force (T_0) of Ca^{2+} -activated isometric contractions (pCa 4.5, temperature 12°C) in control solution (without added Pi; Fig. 1 *A*) and in solution with 10 mM Pi (Fig. 1 *B*). The hs stiffness (k_0) was estimated by the slope of the relation between the force attained at the end of the step and the change in hs length (T_1 relation (38)) (Fig. 1 *C*). The linear fit to the T_1 points shows that k_0 decreases with the [Pi]-dependent decrease in T_0, but less than in proportion to T_0. The abscissa intercept of the regression lines, Y_0 (= T_0/k_0), measures the strain in the hs during the isometric contraction preceding the step. Y_0 decreases with the Pi-dependent reduction in T_0 and k_0 (Table 2 *A*) from 6.8 nm in the solution without added Pi (T_0, 156 kPa and k_0, 23 kPa nm^{-1}) to 5.6 nm in 10 mM Pi (T_0, 90 kPa and k_0, 16 kPa nm^{-1}). The set of experiments done at

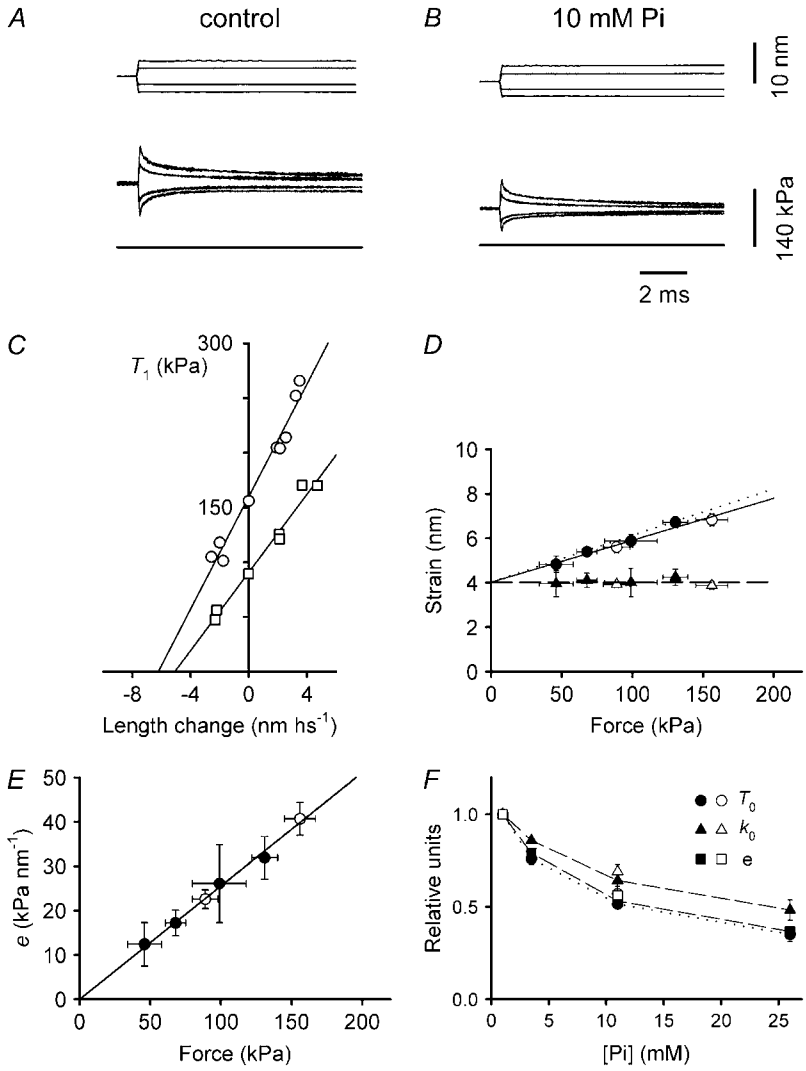

FIGURE 1 Effect of Pi on the hs stiffness. (*A* and *B*) Superimposed force responses (*middle traces*) to step change in hs length (*upper traces*) imposed on an activated fiber (pCa, 4.50) in control solution (*A*) and 10 mM Pi (*B*). The lower trace in each panel is zero force. Fiber length, 4.71 mm; segment length under the striation follower, 1.17 mm; sarcomere length, 2.47 μm; CSA, 3700 μm^2; temperature, 12.4°C. (*C*) T_1 relations in control solution (*circles*) and at 10 mM Pi (*squares*). The relations are obtained by plotting the extreme force attained at the end of the length step, T_1, versus the step size. The lines are the linear regression equations fitted to the experimental points. (*D*) Mean values (± SE) of strain in the hs (Y_0, *circles*) and of the myosin cross-bridges (s_0, *triangles*) plotted against force; data from nine fibers. Pi concentration: solid symbols, 0, 3, 10, and 25 mM added Pi, four fibers from the University of Pennsylvania; open symbols, 0 and 10 mM added Pi, five fibers from the University of Florence. The solid line is fitted by linear regression to the circles, and the dotted line is the linear regression from Fig. 3 *C* in Linari et al. (30). The dashed line is fitted by linear regression to the triangles. (*E*) Relation between the total stiffness of the cross-bridge array in each hs and the steady force modulated by [Pi]. The solid line is a linear regression forced through the origin; solid and open circles as in *D*. (*F*) Pi dependence of isometric force (*circles*), hs stiffness (*triangles*), and stiffness of the cross-bridge array (*squares*), calculated as described in the text. Solid and open symbols as in *D*. Values are plotted relative to their values in control solution. Lines are drawn to join the points (dashed through *triangles* and *squares*, dotted through *circles*).

the University of Pennsylvania, where the range of [Pi] was 3–25 mM, yielded similar results, though the values of force and stiffness for the same [Pi] were slightly lower (Table 2 *B*). The two sets of experiments are merged in Fig. 1 *D*, where Y_0 is plotted versus T_0 for the whole range of [Pi] used (*open circles*: five experiments from the University of Florence; *solid circles*: four experiments from the University of Pennsylvania). The regression line fitted to the pooled data (*solid line* in Fig. 1 *D*) has a slope of 18.9 ± 1.7 nm MPa^{-1} and an ordinate intercept of 4.02 ± 0.18 nm. The slope and the ordinate intercept of the relation do not differ significantly ($p > 0.1$, Student's *t*-test) from the values reported in a previous study (30) as estimates of the compliance of myofilaments (C_f, 21.0 ± 3.3 nm MPa^{-1}) and the average strain of the myosin cross-bridges during the isometric contraction (s, 4.03 ± 0.38 nm), respectively.

This analysis, which was previously explained in detail by Linari et al. (29), is based on a simplification of Eqs. A10 of Ford et al. (40) and A1 of Linari et al. (28) that gives:

$$Y_0 = C_f \cdot T_0 + T_0/(\beta \cdot e_0).$$

In this relation the hs strain is expressed as the sum of the strain of myofilaments, $C_f \cdot T_0$, and that of the cross-bridges, $T_0/(\beta \cdot e_0)$, where $\beta \cdot e_0$ is the stiffness of cross-bridges, given by the product of the stiffness of myosin heads if all heads are attached (e_0) and the fraction of myosin heads that are attached (β). If T_0 changes in proportion to β, then the strain of cross-bridges s ($=T_0/(\beta \cdot e_0)$) remains constant and the change in strain of the hs is explained by the compliance of the myofilaments, as observed in Fig. 1 *D*. At any T_0, and thus at any [Pi], s can be defined by subtracting the strain in the myofilaments ($C_f \cdot T_0$) from the strain in the hs (Y_0) (*triangles* in Fig. 1 *D*). Conversely, the stiffness of the cross-bridges working in parallel in each hs, e ($= \beta \cdot e_0 = T_0/s$), decreases in proportion to the decrease of T_0 by increasing [Pi] (Fig. 1 *E*). In the control solution, e is 40.7 ± 3.7 kPa nm^{-1}(Table 2 *A*), which is not significantly different from the value reported in a previous study under the same conditions (30). These results indicate that the Pi-dependent reduction in T_0 is due to

TABLE 2 Dependence on Pi of isometric force (T_0), hs stiffness (k_0), hs strain (Y_0), cross-bridge stiffness (e), and cross-bridge strain (s)

Added Pi (mM)	T_0 (kPa)	k_0 (kPa nm^{-1})	Y_0 (nm hs^{-1})	e (kPa nm^{-1})	s (nm)
A					
0	156 ± 11	22.8 ± 1.1	6.83 ± 0.27	40.7 ± 3.7	3.87 ± 0.18
10	89 ± 9	15.7 ± 1.0	5.61 ± 0.27	22.6 ± 2.1	3.93 ± 0.14
B					
0	131 ± 9	19.6 ± 1.8	6.71 ± 0.25	31.9 ± 4.8	4.24 ± 0.36
3	99 ± 19	17.0 ± 4.0	5.88 ± 0.29	26.1 ± 8.8	4.01 ± 0.64
10	68 ± 7	12.7 ± 1.7	5.39 ± 0.20	17.2 ± 2.9	4.11 ± 0.32
25	46 ± 12	9.8 ± 3.2	4.83 ± 0.36	12.4 ± 4.9	3.96 ± 0.59

Data are the mean ± SE from five fibers (*A*) and four fibers (*B*), as explained in the text.

a proportional reduction in the number of myosin cross-bridges working in parallel in each hs, without any change in the force per cross-bridge. In Fig. 1 *F* T_0 (*circles*), k_0 (*triangles*), and the number of cross-bridges working in each hs n_0 (*squares*) relative to their values in control solution are plotted as a function of [Pi]. Note that the relative value of n_0 corresponds to the relative stiffness of the array of cross-bridges per hs under the assumption that the unitary stiffness of the attached cross-bridge (ε) is constant independently of the Pi concentration. k_0 (*triangles*) decreases less than T_0 (*circles*) with the increase in Pi (in agreement with previous reports (8,14,15,20)), whereas n_0 (*squares*) reduces with Pi almost exactly as T_0, indicating that the reduction in number of cross-bridges fully accounts for the reduction in the macroscopic isometric force, and the fact that the force per cross-bridge is not affected by changes in [Pi].

Rise of isometric force and stiffness after a period of unloaded shortening

Fig. 2 *A* shows the force development (lower trace) after the end of a period of unloaded shortening in control solution, together with the change in length of the hs (upper trace). The sarcomere length of the fiber in relaxing solution was 2.47 μm. The hs shortening during the 15 ms of unloaded shortening was 60 nm, and during the 500 ms of force development to T_0 it was ~10 nm due to end compliance. On average, in the eight fibers used for this protocol, the shortening during the force development was 16.9 ± 2.5 nm. In Fig. 2 *B*, the time course of force development (*gray*) is fitted by means of a biexponential equation (*solid line*; see Materials and Methods). The amplitudes of the two exponentials, relative to the isometric force (T_0), are $T_F = 0.72 \pm 0.01$ for the fast component (*dot-dashed line*) and $T_S = 0.28 \pm 0.01$ for the slow component (*dashed line*); the rate constants are $r_F = 23.5 \pm 1.7$ s^{-1} and $r_S = 5.4 \pm 0.5$ s^{-1}, respectively.

To measure the change in stiffness of the hs during force development, 4 kHz oscillations were applied either on the isometric force plateau preceding the unloaded shortening or

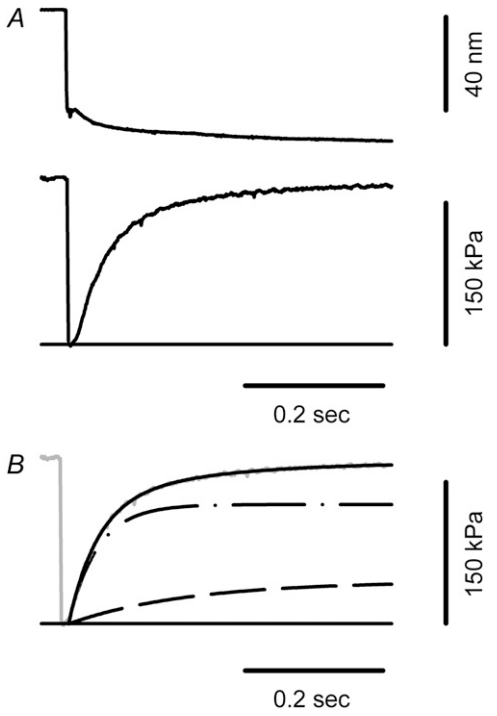

FIGURE 2 Development of force after a period of unloaded shortening. (*A*) Force response (*middle trace*) and corresponding change in length of the hs (*upper trace*). Lower trace is the force baseline. (*B*) Biexponential fit (*solid line*) of force development (*gray*); the fast exponential component is the dot-dashed line, and the slow exponential component is the dashed line. Fiber length, 5.40 mm; average sarcomere length, 2.47 μm; CSA, 6300 μm^2; temperature, 12.3°C.

during the period of force development between 0.25 T_0 and 0.9 T_0 (Fig. 3, *A* and *B*) (see Materials and Methods). As shown in Fig. 3 *C*, the rise in hs stiffness (k_d, *solid squares*) precedes that of force (T_d, *circles*). At $T_d = 0.5$ T_0, k_d is 0.65 k_0, so the time to attain one-half of the isometric plateau value is 25 ms shorter for hs stiffness than for force. In the three fibers used for this protocol, k_d/k_0 rises from 0.44 ± 0.02 at $T_d = 0.25$ T_0 to 0.93 ± 0.01 at 0.84 T_0. The time course of stiffness during force development can also be fitted by means of a biexponential equation. The amplitudes of the two exponentials, relative to the value at the isometric plateau (k_0), are 0.73 ± 0.13 and 0.27 ± 0.12 for the fast and slow components, respectively; the rate constants are $r_{kF} = 36.2 \pm 7.2$ s^{-1} and $r_{kS} = 5.9 \pm 3.5$ s^{-1}.

The strain in the hs during force development (Y_d), calculated by the ratio T_d/k_d, is plotted as a function of T_d in Fig. 3 *D* for the fiber of Fig. 3 *C*, and in Fig. 4 *A* for the mean values from the three fibers used in these experiments (*open circles*). The relation in Fig. 3 *D* is fitted with a linear regression equation that yields a slope of 22.2 ± 1.6 nm MPa^{-1} and an ordinate intercept of 3.80 ± 0.23 nm. The linear fit (*solid line* in Fig. 4 *A*) on the relation obtained from the *open circles* in Fig. 4 *A* yields a slope of 20.5 ± 1.0 nm MPa^{-1} and an ordinate intercept of 3.80 ± 0.23 nm. Both values are not

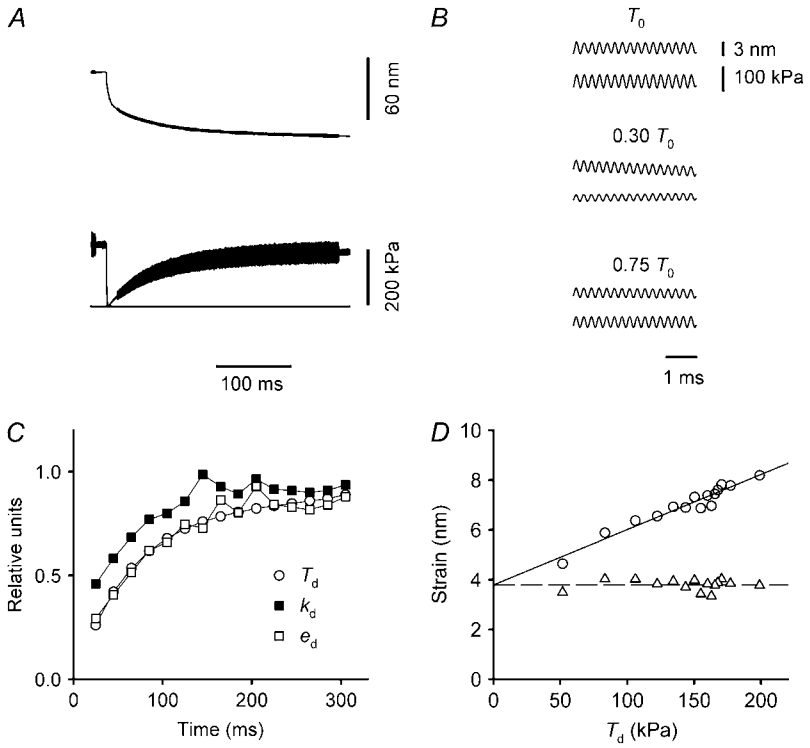

FIGURE 3 Stiffness of the hs during force development. (*A*) Time course of force (*middle trace*) and hs shortening (*upper trace*) during development of force after a period of unloaded shortening. Lower trace is zero force. A 4 kHz sinusoidal length change (± 1.3 nm per hs) is imposed on the fiber when the force trace appears thicker, to estimate the hs stiffness. (*B*) Force and length traces plotted at high speed during the isometric period (T_0, upper frame) preceding the unloaded shortening, at 25 ms (0.3 T_0, middle frame) and at 120 ms (0.75 T_0, lower frame) after the end of unloaded shortening. (*C*) Time course of force (*open circles*), hs stiffness (*solid squares*), and stiffness of the cross-bridge array (*open squares*) during the force development after unloaded shortening. Time zero is the start of shortening. Values are relative to the isometric values before the unloaded shortening. Solid lines are drawn to join the points. (*D*) Strain of the hs (Y_d, *circles*) and cross-bridges (s_d, *triangles*) versus force (T_d) during force development after unloaded shortening. The solid and dashed lines are fitted by linear regression to the circles and triangles, respectively. Fiber length, 3.97 mm; average sarcomere length, 2.53 μm; CSA, 5100 μm^2; temperature, 12.4°C.

significantly different ($p > 0.1$, Student's *t*-test) from those reported as estimates of the compliance of myofilaments (C_f, 21.0 ± 3.3 nm MPa^{-1}) and the average strain of the myosin cross-bridges at the plateau of the isometric contraction (s, 4.03 ± 0.38 nm) in the same conditions of temperature and activation (30). s_d, the strain of the cross-bridges at any time during force development, can be obtained by subtracting the filament strain ($C_f \cdot T_d$) from the hs strain (Y_d) (*open triangles* in Figs. 3 *D* and 4 *A*). s_d is independent of the time and the level of force. Consequently, i, the ratio T_d/s_d, that expresses the total stiffness of myosin cross-bridges in the hs during force development (e_d), rises in proportion to T_d, and *ii*, the rise in the number of cross-bridges attached to actin relative to the number attached at the plateau of the isometric contraction (n_d/n_0) measured by the rise of the ratio e_d/e, practically superimposes on the rise of isometric force (open squares in Figs. 3 *C* and 4 *B*). From this analysis we conclude that the average force per cross-bridge is the same at any time during the force development and we exclude the possibility that generation of force lags behind stiff attachment of the cross-bridges by more than a millisecond (see also Brunello et al. (41)).

Effect of Pi on the rise of isometric force and stiffness

The effect of 10 mM Pi on the time course of force development after a period of unloaded shortening is shown in Fig. 5. The reduction of isometric force by Pi (Figs. 5 *A* and 6 *A*) is accompanied by an increase in the rate constant of force development (Fig. 5 *B*). As in control solution, the time course of force development could be fitted with a biexponential equation. The dependence on [Pi] of the amplitudes and the rate constants of the fast and slow exponential components is shown in Fig. 6, *B* and *C*, respectively. The relative amplitudes of the two components are not significantly affected by Pi in the range of concentrations used (0–20 mM added Pi, eight fibers). The rate constant of the fast component r_F (*circles* in Fig. 6 *C*) increases monotonically with [Pi], whereas the rate constant of the slow component r_S (*triangles*) decreases with [Pi]. This is reminiscent of the dependence on Pi of the two phases of force recovery after a pressure jump (22). The effect of change in [Pi] on r_F decreases at higher Pi concentrations: at 10 mM Pi, r_F is 70% larger than the control value and it increases further by only 30% between 10 and 20 mM Pi. A limit in the Pi-dependent enhancement of r_F is expected according to the idea that force generation is a relatively slow process that occurs before a relatively fast Pi release (7,12,14,21,22). According to this mechanism, the zero-force state AM-ADP-Pi, in rapid equilibrium with the detached state M-ADP-Pi, is followed by two strongly bound force-generating states, AM'-ADP-Pi and AM'-ADP, according to Scheme 2:

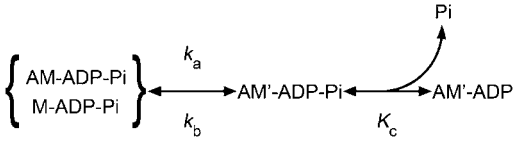

where k_a and k_b are the forward and backward rate constants for the force-generating transition, and K_C is the equilibrium

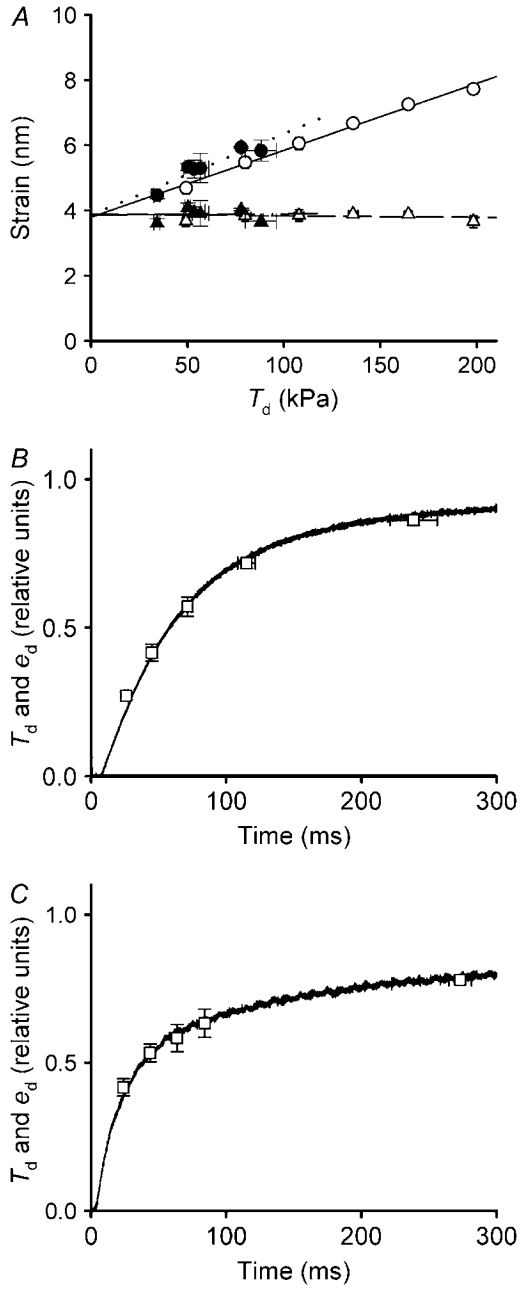

FIGURE 4 Effect of Pi on the stiffness during force development. (*A*) Strain of the hs (*circles*) and cross-bridges (triangles) versus force in control solution (*open symbols*) and in solution with 10 mM Pi (*solid symbols*). Lines are fitted to the open circles (*solid line*), solid circles (*dotted line*), open triangles (*dashed line*), and solid triangles (*dot-dashed line*). (*B* and *C*) Time course of force (*trace*) and stiffness of the cross-bridge array (*open squares*) in control solution (*B*) and at 10 mM Pi (*C*). Values are relative to the isometric values before the unloaded shortening. Time zero is the start of shortening. Mean values (± SE) from three fibers.

constant that defines the rapid Pi release step. With this scheme the Pi dependence of r_F can be described by the following equation (14):

$$r_F = k_a + k_b[\mathrm{Pi}]/(K_C + [\mathrm{Pi}]). \quad (2)$$

Fitting Eq. 2 to the r_F data (*dashed line* in Fig. 6 *C*), we obtain $k_a = 21.2 \pm 0.96\ s^{-1}$; $k_b = 66.4 \pm 12.6\ s^{-1}$; and $K_C = 28.9 \pm 9.8$ mM.

The effect of [Pi] on the rise of stiffness during force development after unloaded shortening was investigated by repeating the 4 kHz oscillation protocol in test solution with 10 mM Pi. The dependence of the hs strain Y_d on the force T_d is shown by solid circles in Fig. 4 *A* (means from the same three fibers as *open circles*). The linear fit to the points yields a slope of 24.5 ± 4.5 nm MPa^{-1} and an ordinate intercept of 3.86 ± 0.30 nm. The two estimates are not significantly different ($p > 0.1$, Student's *t*-test) from the estimates of the compliance of myofilaments (C_f, 21.0 ± 3.3 nm MPa^{-1}) and the average strain of the myosin cross-bridges at the plateau of the isometric contraction (*s*, 4.03 ± 0.38 nm) (30), respectively. Consequently, during force development in 10 mM Pi, the strain of the cross-bridges (s_d, *solid triangles* in Fig. 4 *A*) does not change with force and the increase in the number of actin attached cross-bridges relative to those at T_0 (*squares* in Fig. 4 *C*) has the same time course as the rise in the isometric force, even though the rate constant of the process leading to force development is increased by 70%.

DISCUSSION

In this work, we investigated the relation between chemical and mechanical steps of the cyclic reaction of skeletal muscle myosin with actin that leads to isometric force generation and ATP splitting in situ. For this we used fast-sarcomere-level mechanics on demembranated fibers of rabbit psoas to determine how [Pi] modulates the number and force of actin-attached myosin cross-bridges during transient and steady-state conditions of isometric contraction.

Effect of Pi on the force and number of myosin cross-bridges during steady isometric contraction

At the plateau of isometric contraction in control solution, the hs stiffness is 22.8 ± 1.1 kPa nm^{-1} (Table 2 *A*) and that of the array of myosin cross-bridges in the hs (*e*) is 40.7 ± 3.7 kPa nm^{-1} (Table 2 *A*). Increasing [Pi] decreases *e* in proportion to the isometric force (Fig. 1 *E*). Thus the mass action of [Pi] decreases the macroscopic force and the number of cross-bridges rigidly attached to actin by the same amount, so that the force of the cross-bridge is not altered by [Pi]. It must be noted here that the same conclusion was drawn by Kawai and Halvorson (21) based on their result that, in contrast to all the other studies, the force and the fiber stiffness are reduced in proportion by increasing [Pi]. However, their result is contradicted by the finding here that it is the stiffness of the motor array that is decreased in proportion to force when [Pi] is increased. Their result was probably obtained because they used sinusoidal length changes at frequencies up to 350 Hz (more than 10-fold lower than that used here) and extrapo-

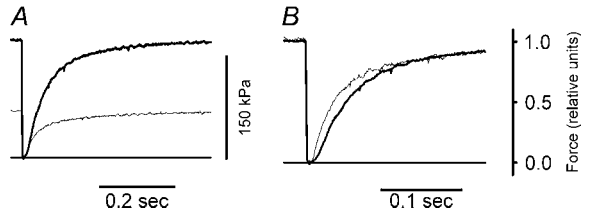

FIGURE 5 Effect of Pi on the time course of force development after a period of unloaded shortening. (*A*) Superimposed force responses in control solution (*thick trace*) and at 10 mM Pi (*thin trace*). (*B*) Superimposed force responses as in *A* after normalization for their respective isometric plateau force. Same fiber as in Fig. 2.

lated to infinite frequency. Based on the known rate of quick recovery and experimentally determined mechanical compliances, this procedure would greatly underestimate the stiffness at high [Pi].

Our study allows us to conclude that the effect of increasing [Pi] on the force and number of cross-bridges is similar to that of decreasing [Ca^{2+}] (30). The difference between increasing in [Pi] and decreasing [Ca^{2+}] observed by Regnier et al. (15) appears to be related to a stiffness-force relation at different [Ca^{2+}] that is much closer to the line of identity (see Fig. 1 *B* of Regnier et al. (15)). A similar result was also found by Kagawa et al. (42), but it is questionable because myofilament compliance was not taken into account. Moreover, we exclude the kinetic relevance of a stiff, zero-force AM*.ADP.Pi cross-bridge (see Introduction) (15) generated by the isomerization of the weakly bound A-M.ADP.Pi cross-bridge. Thus the six-step reaction scheme of Regnier et al. (15) is reduced to a five-step reaction scheme similar to that of Kawai and Halvorson (21) and Dantzig et al. (14):

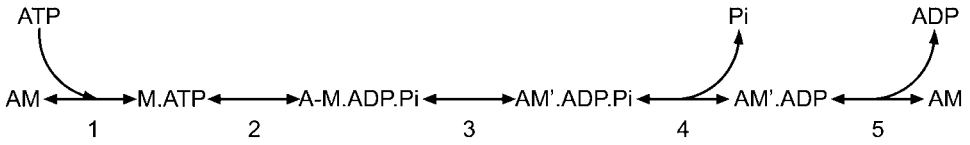

Scheme 3

where the strongly bound AM'.ADP.Pi cross-bridge formed via step 3 from the weakly bound A-M.ADP.Pi state is also able to generate force directly or after no more than 1 ms or so. Rapid force generation after cross-bridge attachment is expected based on the theory of Huxley and Simmons (38), which postulates that force is the result of the rapid equilibrium (1000 s^{-1}) between different force generating states of the attached cross-bridges, and in agreement with previous findings in intact fibers from frog skeletal muscle (41). Note that the assumption of the Huxley and Simmons model for force generation implies the presence of several (mechanically relevant) states not shown on the biochemical schemes. This is because the biochemical schemes only show the states between which the rate transitions are relevant for the kinetics studied in this work. Our simplification implies that AM'.ADP.Pi and AM'.ADP states are composed of several mechanical states in rapid equilibrium.

The idea of a rapid attainment of the equilibrium distribution between force-generating states of the cross-bridges is also supported by the finding that, during isometric force development, the rise in the number of myosin cross-bridges attached to actin and the force (T_d) have the same time course (Figs. 3 *C* and 4 *B*). This result implies that the average force per cross-bridge is the same at any time during the rise of T_d, excluding a significant delay (>1 ms) between generation of stiffness and generation of force by the cross-bridge.

Note that this conclusion is not contradicted by the finding that alterations of temperature change the isometric force by changing the equilibrium distribution of cross-bridges between low-force and high-force states (30,43,44). From the temperature experiments in rabbit psoas fibers (30), we concluded that the isometric force at 12°C (the temperature of the experiments presented here) is ~75% of the maximum force attained when all cross-bridges are in the high-force state. In terms of kinetics Scheme 3, this means that both AM'.ADP.Pi and AM'.ADP represent a similar proportion of low- (25%) and high- (75%) force states in rapid equilibrium. The partition between low- and high-force states is altered by changes in temperature but not by changes in [Pi].

Effect of Pi on the rise of isometric force and identification of the rate-limiting step for force generation

The number of attached cross-bridges is proportional to force (Fig. 4, *B* and *C*). Thus the rate constants for the development of isometric force and the rise in the number of attached cross-bridges are the same. It follows that the increase of rate constant for rise of force with increase of [Pi] (Fig. 6 *C*) applies equally to the rate constant for number of attached cross-bridges. The effect reduces at high [Pi] (Fig. 6 *C*). These effects, reported previously for the isometric force (15,17–19,21,22), are explained by the mass action of Pi on the equilibrium distribution among the various states of the cross-bridge and by the assumption that generation of force in the cross-bridge precedes Pi release (14,21,22). A similar kinetic effect of Pi was reported for the rate constant of force transient (r_{Pi}) after a jump in [Pi] (12,14,15,17–19). However, for the same [Pi], the value of r_F is lower than that of r_{Pi} (15). Accordingly, the values of r_F reported here for force development after shortening at [Pi] larger than 5 mM are ~1/2 the values of r_{Pi} previously found for Pi transients by

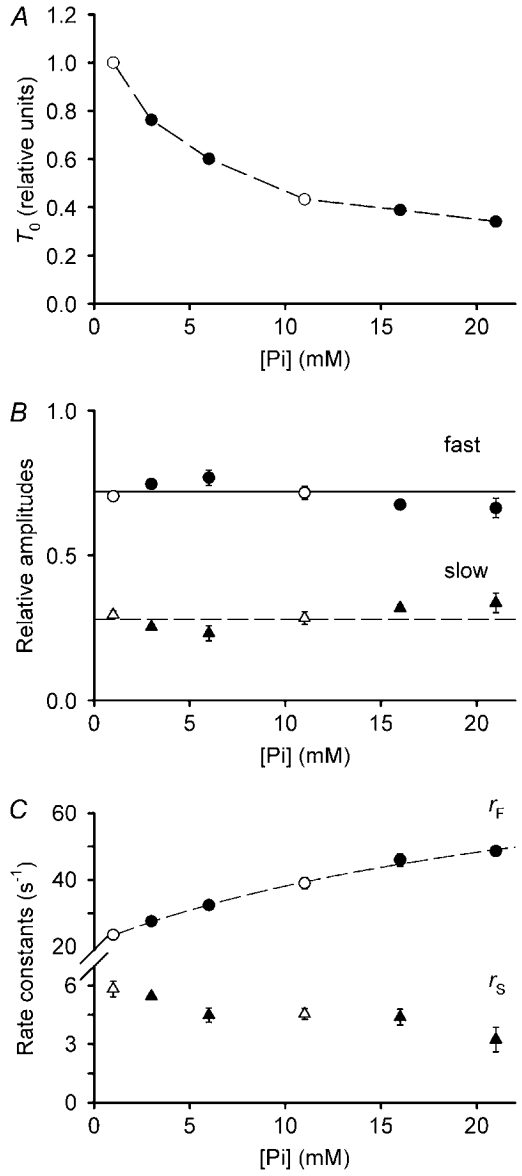

FIGURE 6 Effect of Pi on the rate of force development after unloaded shortening. (*A*) Pi dependence of isometric force. (*B*) Relative amplitudes of the slow (*triangles*) and fast (*circles*) exponential components. The lines are the mean values of the relative amplitudes for the slow (*dashed*) and fast (*solid*) components. (*C*) Pi-dependence of the rate constants of the slow (*triangles*) and fast (*circles*) exponential components. The ordinate scale is split to clarify the changes of r_F and r_S. The dashed line is the fit of Eq. 2 to the data (see text). In all graphs, values are mean (± SE): open symbols, from eight fibers; solid symbols, from three fibers. Absence of bars indicates an error smaller than the symbol.

two of the authors (14). We propose that the difference between the two rate constants is due to the lag introduced in the rate of force development after unloaded shortening by a relatively slow transition occurring before the step leading to the stiff force-generating state of the cross-bridge. In agreement with this view, Eq. 2, fitted to the r_F-Pi relation in Fig. 6 *C*, provides a value for the rate constant of the force-generating step at saturating Pi ($k_a + k_b$) of (21.2 + 66.4 =) 87.6 s^{-1} and a $K_C \sim 30$ mM, whereas in Dantzig et al. (14) the same equation, fitted to the r_{Pi}-Pi relation, provides an estimate of ($k_a + k_b$) of (21.1 + 102.3 =) 123.4 s^{-1} and $K_C \sim 10$ mM. This difference can be explained in the six-step reaction scheme (Scheme 1) of Regnier et al. (15) by assuming that whereas the Pi transient is rate limited only by step 4, de novo force generation is rate limited by two sequential steps: step 3, leading to a strongly bound state generating stiffness but no force, and step 4, leading to the force generating state. Our finding that there is no lag between the formation of strongly bound cross-bridges and generation of force reduced Scheme 1 to Scheme 3, where the lag that explains why de novo force generation is slower than the Pi transient must be assigned to the ATP hydrolysis step or other transitions included in step 2. This conclusion supports the five-step kinetic scheme of Sleep et al. (23), in which, taking into account measurements in solution and in myofibrils (45,46), the rate of the hydrolysis step (step 2) is assumed to be slower than in the kinetic scheme of Regnier et al. (15). Using the Q_{10} (5.5) calculated from the rate constants reported by Sleep et al. (23) at 20°C and 5°C, the rate constants of the hydrolysis step at the temperature of our experiments (11°C) should be ~25/s (forward) and ~15/s (backward), which is a factor of 2 smaller than the values assumed by Regnier et al. (15) and adequate to explain the difference between r_F and r_{Pi}.

The kinetic reaction scheme presented by Sleep and coworkers (23,47) also implies that, according to solution measurements (48) and fiber measurements (49), the Pi release step (step 4 in Scheme 3) is a relatively slow process that follows the fast force-generating transition (step 3 in Scheme 3). This conclusion seems inconsistent with the results of this work because if Pi release is rate limiting, the progressive reduction of the Pi effect on the rate of force development at high [Pi] would occur with much higher values of r_F than observed. Moreover, a relatively slow Pi release step after a fast force-generation step is inconsistent with the asymptotic shape of the relation between r_{Pi} and [Pi] (14).

Effect of Pi on the ATPase rate in the isometric contraction

In fibers from fast skeletal muscle, the ATPase rate is reduced by Pi less than in proportion to the reduction of isometric force (8,10,50–53). This is not expected because the shift of the equilibrium of step 4 in Scheme 3 toward the AM'.ADP.Pi state by mass action of [Pi] reduces the flux through the whole cycle. To resolve the discrepancy, it was hypothesized (54) that the effect of Pi on the reverse rate constant of Pi release depends on the strain in the cross-bridge, and thus the rate would be higher at larger strain. In this way an increase in [Pi] would produce a greater effect on the total force than on the number of cross-bridges and thus on the ATPase rate. This idea is contradicted by the evidence presented here that the reduction of macroscopic force by Pi is proportional to the reduction in the number of cross-

bridges, without change in the force per cross-bridge. Thus the increase in [Pi] reduces the number of stiffness- and force-generating cross-bridges more than the ATPase rate. This conclusion implies, as a corollary, that the ATP splitting rate per attached cross-bridge is elevated by the increase in [Pi].

The authors thank Gabriella Piazzesi for continuous discussions during the preparation of this work, and Corrado Poggesi, Malcolm Irving, and Chiara Tesi for helpful criticisms of the manuscript. We also thank Alessandro Aiazzi and Mario Dolfi for skilled technical assistance.

This research was supported by the National Institutes of Health (grant R01AR49033), the Ministero dell'Università e della Ricerca (MIUR-COFIN 2006), the Istituto di Tecnologie Biomediche (ITB-CNR) and the Ente Casa di Risparmio di Firenze.

REFERENCES

1. Lymn, R. W., and E. W. Taylor. 1971. Mechanism of adenosine triphosphate hydrolysis by actomyosin. *Biochemistry.* 10:4617–4624.
2. Rayment, I. H. M. Holden, M. Whittaker, C. B. Yohn, M. Lorenz, K. C. Holmes and R. A. Milligan. 1993. Structure of the actin-myosin complex and its implications for muscle contraction. *Science.* 261:58–65.
3. Geeves, M. A., and K. C. Holmes. 2005. The molecular mechanism of muscle contraction. *Adv. Protein Chem.* 71:161–193.
4. Nyitrai, M., and M. A. Geeves. 2004. Adenosine diphosphate and strain sensitivity in myosin motors. *Philos. Trans. R. Soc. Lond. B Biol. Sci.* 359:1867–1877.
5. Brandt, P. W., R. N. Cox, M. Kawai, and T. Robinson. 1982. Regulation of tension in skinned muscle fibers. Effect of cross-bridge kinetics on apparent Ca2+ sensitivity. *J. Gen. Physiol.* 79:997–1016.
6. Pate, E., and R. Cooke. 1985. The inhibition of muscle contraction by adenosine 5′ (beta, gamma-imido) triphosphate and by pyrophosphate. *Biophys. J.* 47:773–780.
7. Hibberd, M. G., J. A. Dantzig, D. R. Trentham, and Y. E. Goldman. 1985. Phosphate release and force generation in skeletal muscle fibers. *Science.* 228:1317–1319.
8. Kawai, M., K. Guth, K. Winnikes, C. Haist, and J. C. Ruegg. 1987. The effect of inorganic phosphate on the ATP hydrolysis rate and the tension transients in chemically skinned rabbit psoas fibers. *Pflugers Arch.* 408:1–9.
9. Brozovich, F. V., L. D. Yates, and A. M. Gordon. 1988. Muscle force and stiffness during activation and relaxation. *J. Gen. Physiol.* 91:399–420.
10. Cooke, R., K. Franks, G. B. Luciani, and E. Pate. 1988. The inhibition of rabbit skeletal muscle contraction by hydrogen ions and phosphate. *J. Physiol.* 395:77–97.
11. Pate, E., and R. Cooke. 1989. Addition of phosphate to active muscle fibers probes actomyosin states within the powerstroke. *Pflugers Arch.* 414:73–81.
12. Millar, N. C., and E. Homsher. 1990. The effect of phosphate and calcium on force generation in glycerinated rabbit skeletal muscle fibers. A steady-state and transient kinetic study. *J. Biol. Chem.* 265:20234–20240.
13. Martyn, D. A., and A. M. Gordon. 1992. Force and stiffness in glycerinated rabbit psoas fibers. Effects of calcium and elevated phosphate. *J. Gen. Physiol.* 99:795–816.
14. Dantzig, J. A., Y. E. Goldman, N. C. Millar, J. Lacktis, and E. Homsher. 1992. Reversal of the cross-bridge force-generating transition by photogeneration of phosphate in rabbit psoas muscle fibres. *J. Physiol.* 451:247–278.
15. Regnier, M., C. Morris, and E. Homsher. 1995. Regulation of the cross-bridge transition from a weakly to strongly bound state in skinned rabbit muscle fibers. *Am. J. Physiol.* 269:C1532–C1539.
16. Kawai, M. 1986. The role of orthophosphate in crossbridge kinetics in chemically skinned rabbit psoas fibres as detected with sinusoidal and step length alterations. *J. Muscle Res. Cell Motil.* 7:421–434.
17. Walker, J. W., Z. Lu, and R. L. Moss. 1992. Effect of Ca^{2+} on the kinetics of phosphate release in skeletal muscle. *J. Biol. Chem.* 267:2459–2466.
18. Tesi, C., F. Colomo, S. Nencini, N. Piroddi, and C. Poggesi. 2000. The effect of inorganic phosphate on force generation in single myofibrils from rabbit skeletal muscle. *Biophys. J.* 78:3081–3092.
19. Tesi, C., F. Colomo, S. Nencini, N. Piroddi, and C. Poggesi. 2002. Characterization of the cross-bridge force-generating step using inorganic phosphate and BDM in myofibrils from rabbit skeletal muscles. *J. Physiol.* 541:187–199.
20. Chase, P. B., D. A. Martyn, M. J. Kushmerick, and A. M. Gordon. 1993. Effects of inorganic phosphate analogues on stiffness and unloaded shortening of skinned muscle fibres from rabbit. *J. Physiol.* 460:231–246.
21. Kawai, M., and H. R. Halvorson. 1991. Two step mechanism of phosphate release and the mechanism of force generation in chemically skinned fibers of rabbit psoas muscle. *Biophys. J.* 59:329–342.
22. Fortune, N. S., M. A. Geeves, and K. W. Ranatunga. 1991. Tension responses to rapid pressure release in glycerinated rabbit muscle fibers. *Proc. Natl. Acad. Sci. USA.* 88:7323–7327.
23. Sleep, J., M. Irving, and K. Burton. 2005. The ATP hydrolysis and phosphate release steps control the time course of force development in rabbit skeletal muscle. *J. Physiol.* 563:671–687.
24. Huxley, H. E., A. Stewart, H. Sosa, and T. Irving. 1994. X-ray diffraction measurements of the extensibility of actin and myosin filaments in contracting muscle. *Biophys. J.* 67:2411–2421.
25. Wakabayashi, K., Y. Sugimoto, H. Tanaka, Y. Ueno, Y. Takezawa, and Y. Amemiya. 1994. X-ray diffraction evidence for the extensibility of actin and myosin filaments during muscle contraction. *Biophys. J.* 67:2422–2435.
26. Higuchi, H., T. Yanagida, and Y. E. Goldman. 1995. Compliance of thin filaments in skinned fibers of rabbit skeletal muscle. *Biophys. J.* 69:1000–1010.
27. Dobbie, I., M. Linari, G. Piazzesi, M. Reconditi, N. Koubassova, M. A. Ferenczi, V. Lombardi, and M. Irving. 1998. Elastic bending and active tilting of myosin heads during muscle contraction. *Nature.* 396:383–387.
28. Linari, M., I. Dobbie, M. Reconditi, N. Koubassova, M. Irving, G. Piazzesi, and V. Lombardi. 1998. The stiffness of skeletal muscle in isometric contraction and rigor: the fraction of myosin heads bound to actin. *Biophys. J.* 74:2459–2473.
29. Linari, M., R. Bottinelli, M. A. Pellegrino, M. Reconditi, C. Reggiani, and V. Lombardi. 2004. The mechanism of the force response to stretch in human skinned muscle fibres with different myosin isoforms. *J. Physiol.* 554:335–352.
30. Linari, M., M. Caremani, C. Piperio, P. Brandt, and V. Lombardi. 2007. Stiffness and fraction of myosin motors responsible for active force in permeabilized muscle fibers from rabbit psoas. *Biophys. J.* 92:2476–2490.
31. Dantzig, J. A., Y. E. Goldman, and V. Lombardi. 1991. Tension transients following sudden length changes in the presence and absence of inorganic phosphate in single rabbit psoas muscle fibers. 1991. *Biophys. J.* 59:36a. (Abstr.)
32. Linari, M., A. Aiazzi, M. Dolfi, G. Piazzesi, and V. Lombardi. 1993. A system for studying tension transients in short segments of skinned muscle fibres from rabbit psoas. *J. Physiol.* 473:8P. (Abstr.)
33. Goldman, Y. E., M. G. Hibberd, and D. R. Trentham. 1984. Relaxation of rabbit psoas muscle fibres from rigor by photochemical generation of adenosine-5′-triphosphate. *J. Physiol.* 354:577–604.
34. Lombardi, V., and G. Piazzesi. 1990. The contractile response during steady lengthening of stimulated frog muscle fibres. *J. Physiol.* 431:141–171.
35. Huxley, A. F., and V. Lombardi. 1980. A sensitive force transducer with resonant frequency 50 kHz. *J. Physiol.* 305:15–16.
36. Goldman, Y. E. 1987. Measurement of sarcomere shortening in skinned fibers from frog muscle by white light diffraction. *Biophys. J.* 52:57–68.
37. Huxley, A. F., V. Lombardi, and D. Peachey. 1981. A system for fast recording of longitudinal displacement of a striated muscle fibre. *J. Physiol.* 317:12–13.

38. Huxley, A. F., and R. M. Simmons. 1971. Proposed mechanism of force generation in striated muscle. *Nature*. 233:533–538.

39. Brandt, P. W., J. P. Reuben, and H. Grundfest. 1972. Regulation of tension in the skinned crayfish muscle fiber. II. Role of calcium. *J. Gen. Physiol*. 59:305–317.

40. Ford, L. E., A. F. Huxley, and R. M. Simmons. 1981. The relation between stiffness and filament overlap in stimulated frog muscle fibres. *J. Physiol*. 311:219–249.

41. Brunello, E., P. Bianco, G. Piazzesi, M. Linari, M. Reconditi, P. Panine, T. Narayanan, W. I. Helsby, M. Irving, and V. Lombardi. 2006. Structural changes in the myosin filament and cross-bridges during active force development in single intact frog muscle fibres: stiffness and X-ray diffraction measurements. *J. Physiol*. 577:971–984.

42. Kagawa, K., K. Horiuti, and K. Yamada. 1995. BDM compared with Pi and low Ca^{2+} in the cross-bridge reaction initiated by flash photolysis of caged ATP. *Biophys. J*. 69:2590–2600.

43. Piazzesi, G., M. Reconditi, N. Koubassova, V. Decostre, M. Linari, L. Lucii, and V. Lombardi. 2003. Temperature dependence of the force-generating process in single fibres from frog skeletal muscle. *J. Physiol*. 549:93–106.

44. Decostre, V., P. Bianco, V. Lombardi, and G. Piazzesi. 2005. Effect of temperature on the working stroke of muscle myosin. *Proc. Natl. Acad. Sci. USA*. 102:13927–13932.

45. Ma, Y. Z., and E. W. Taylor. 1994. Kinetic mechanism of myofibril ATPase. *Biophys. J*. 66:1542–1553.

46. Herrmann, C., C. Lionne, F. Travers, and T. Barman. 1994. Correlation of ActoS1, myofibrillar, and muscle fiber ATPases. *Biochemistry*. 33:4148–4154.

47. Smith, D. A., and J. Sleep. 2004. Mechanokinetics of rapid tension recovery in muscle: the myosin working stroke is followed by a slower release of phosphate. *Biophys. J*. 87:442–456.

48. White, H. D., B. Belknap, and M. R. Webb. 1997. Kinetics of nucleoside triphosphate cleavage and phosphate release steps by associated rabbit skeletal actomyosin, measured using a novel fluorescent probe for phosphate. *Biochemistry*. 36:11828–11836.

49. He, Z. H., R. K. Chillingworth, M. Brune, J. E. Corrie, D. R. Trentham, M. R. Webb, and M. A. Ferenczi. 1997. ATPase kinetics on activation of rabbit and frog permeabilized isometric muscle fibres: a real time phosphate assay. *J. Physiol*. 501:125–148.

50. Webb, M. R., M. G. Hibberd, Y. E. Goldman, and D. R. Trentham. 1986. Oxygen exchange between Pi in the medium and water during ATP hydrolysis mediated by skinned fibers from rabbit skeletal muscle. Evidence for Pi binding to a force-generating state. *J. Biol. Chem*. 261:15557–15564.

51. Bowater, R., and J. Sleep. 1988. Demembranated muscle fibers catalyze a more rapid exchange between phosphate and adenosine triphosphate than actomyosin subfragment 1. *Biochemistry*. 27:5314–5323.

52. Potma, E. J., I. A. van Grass, and G. J. Stienen. 1995. Influence of inorganic phosphate and pH on ATP utilization in fast and slow skeletal muscle fibers. *Biophys. J*. 69:2580–2589.

53. Potma, E. J., and G. J. Stienen. 1996. Increase in ATP consumption during shortening in skinned fibres from rabbit psoas muscle: effects of inorganic phosphate. *J. Physiol*. 496:1–12.

54. Pate, E., and R. Cooke. 1989. A model of crossbridge action: the effects of ATP, ADP and Pi. *J. Muscle Res. Cell Motil*. 10:181–196.